Condensate, momentum distribution, and final-state effects in liquid ^{4}He

H. R. Glyde
Department of Physics and Astronomy, University of Delaware, Newark, Delaware 19716

R. T. Azuah and W. G. Stirling
Department of Physics, Oliver Lodge Laboratory, University of Liverpool, Liverpool L69 3BX, United Kingdom

(Received 15 February 2000)

We present benchmark, high precision measurements of the dynamic structure factor $J(Q,y)$ of liquid ^{4}He at several temperatures over a wide wave vector transfer range $15 \leqslant Q \leqslant 29$ Å^{-1}. $J(Q,y)$ is very different in the superfluid phase below T_λ and in the normal phase above T_λ where $T_\lambda = 2.17$ K. Below T_λ, $J(Q,y)$ contains a pronounced additional contribution near $y=0$ that is asymmetric about $y=0$, reflecting a condensate contribution modified by asymmetric final-state (FS) effects. The asymmetry in $J(Q,y)$ is direct qualitative evidence of a condensate. We analyze the data at all T using the same model of $J(Q,y)$ consisting of a condensate fraction n_0, a momentum distribution $n^*(\mathbf{k})$ for states $k>0$ above the condensate, and a FS broadening function $R(Q,y)$. We find a condensate fraction given by $n_0(T) = n_0(0)[1-(T/T_\lambda)^\gamma]$ with $n_0(0) = (7.25 \pm 0.75)\%$ and $\gamma = 5.5 \pm 1.0$ for $T < T_\lambda$, which is 30% below existing observed values, and $n_0 = (0 \pm 0.3)\%$ for $T > T_\lambda$. We determine $n(k)$ in both phases. The $n^*(\mathbf{k})$ is significantly narrower than a Gaussian in both superfluid and normal ^{4}He and narrowest in the normal phase. The final-state function is determined from the data and is the same within precision above and below T_λ. The precise form of $R(Q,y)$ is important in determining the value of $n_0(T)$ below T_λ. When independent, theoretical $R(Q,y)$ are used in the analysis, the $n_0(T)$ is found to be the same as or smaller than the above value.

I. INTRODUCTION

Superfluidity and Bose-Einstein condensation (BEC) in Bose gases and liquids are a topics of great current interest. Superfluidity in liquid ^{4}He has a long and rich history of study[1–8] and BEC has recently been demonstrated spectacularly in dilute Bose gases.[9–13] Einstein[14] first showed that a gas of particles obeying the statistics proposed by Bose[15] could condense into a state having macroscopic occupation of a single-particle quantum state (BEC) below a critical temperature T_c. In the 1930s superfluidity was discovered in[1–3] liquid ^{4}He below a temperature $T_\lambda = 2.17$ K. London[16] proposed that this superfluidity was associated with BEC with $T_\lambda = T_c$.

Superfluidity can be readily demonstrated in liquid ^{4}He today. However, because liquid ^{4}He is a strongly interacting fluid, the fraction of the fluid condensed in the zero momentum state is small,[17–20,8] less than 10%. For this reason and also because of the strong interaction,[21,22] BEC in superfluid ^{4}He is difficult to observe. Measurements to date[6,7] are summarized below. Unambiguous identification of a condensate in liquid ^{4}He and accurate determination of the condensate fraction $n_0(T)$ remain important goals today.

In contrast, BEC has been unambiguously demonstrated in dilute gases of trapped alkali-metal atoms.[9–12] In this case, the gas is dilute and weakly interacting so that nearly 100% of the gas is condensed into the lowest single particle state at low T. These condensed gases show remarkable properties but superfluidity, stable persistent flow, is difficult to demonstrate. Clear observation of superfluidity in trapped Bose gases is an important research goal today.

The aim of the present investigation is to determine the condensate fraction $n_0(T)$, the momentum distribution $n(\mathbf{k})$, and the final-state function $R(Q,y)$ in liquid ^{4}He accurately as a function of temperature. The most direct method to observe $n_0(T)$ is by neutron inelastic scattering at high energy ($\hbar\omega$) and momentum ($\hbar Q$) transfer.[23,24] The quantity observed is the dynamic structure factor (DSF) $S(Q,\omega)$.[6,7] At high ω and Q, $S(Q\omega)$ depends on single-atom properties and the energy transfer ω is Doppler broadened by the atomic momentum distribution $n(\mathbf{k})$. From this broadening, $n(\mathbf{k})$ is measured and $n_0(T)$ is determined.

Specifically, provided there are no perfectly hard core interactions, $S(Q,\omega)$ at $Q \to \infty$ reduces to the impulse approximation[6] (IA),

$$S_{IA}(Q,\omega) = \int d\mathbf{k} n(\mathbf{k}) \delta(\omega - \omega_R - \mathbf{v}_R \cdot \mathbf{k}), \qquad (1)$$

where $\hbar\mathbf{k}$ is the ^{4}He atom momentum in the fluid, $n(\mathbf{k})$ is the momentum distribution, and $\hbar\omega_R = \hbar^2 Q^2/2m$ and $\mathbf{v}_R = \hbar\mathbf{Q}/m$ are the free ^{4}He atom recoil energy and velocity, respectively. $S_{IA}(Q,\omega)$ depends solely on $n(\mathbf{k})$.

At finite Q, interactions of the recoiling atom with its neighbors, denoted final-state (FS) effects, contribute to $S(Q,\omega)$. The observed $S(Q,\omega)$ is then[21,6,7]

$$S(Q,\omega) = \int d\omega' S_{IA}(Q,\omega') R(Q,\omega-\omega'). \qquad (2)$$

Equation (2) may be regarded as the definition[21] of the FS broadening function $R(Q,\omega)$. At finite Q (e.g., $Q \simeq 20$ Å^{-1}) $R(Q,\omega)$ has a significant width and $R(Q,\omega) \to \delta(\omega)$ as $Q \to \infty$.

When there is a condensate, $n(\mathbf{k})$ contains a term $n_0\delta(\mathbf{k})$. This term leads to a term $S_{IA}(Q,\omega) = n_0\delta(\omega-\omega_R)$ in the IA

 ©2000 The American Physical Society

in Eq. (1) and a term $S(Q,\omega)=n_0R(Q,\omega-\omega_R)$ in the observed DSF in Eq. (2). $S(Q,\omega)$ is conveniently expressed in terms of the y-scaling variable $y=(\omega-\omega_R)/v_R$ and the function $J(Q,y)\equiv v_RS(Q,\omega)$, which peaks at $y=0$ and is approximately independent of Q. In $J(Q,y)$ the term arising from the condensate is

$$n_0R(Q,y). \tag{3}$$

A specific goal here is to demonstrate that the $n_0R(Q,y)$ term can be observed in the data and is a direct signature of the condensate.

Measurement of $n_0(T)$ by neutron scattering has a long history, which is reviewed by Sokol,[25] Glyde,[6] Silver and Sokol,[26] Glyde and Svensson,[27] Svensson and Sears,[28] Svensson,[29] and others. Early measurements, discussed by Martel *et al.*,[30] produced a wide range of n_0 values, $2\% \leqslant n_0 \leqslant 17\%$. Sears *et al.*[31] developed a method for treating FS effects based on an additive expansion[22] of $R(Q,\omega)$, which led to the first consistent values of n_0. With this method Sears *et al.*[31] and Mook[32] obtained $n_0(0)=(13.9\pm2.3)\%$, and $n_0(0)=(11\pm3)\%$, respectively. In pioneering measurements using the IPNS spallation neutron source to go to higher Q values and analyzing the data using the convolution[21] form (2) of $S(Q\omega)$ with the FS function calculated by Silver,[33,26] Sokol and collaborators[25,34–37] obtain $n_0=10.0\pm1.25\%$ at low temperature (0.35 K).

In this study, we take advantage of the high flux ISIS neutron scattering facility and the MARI instrument at Rutherford Appleton Laboratory to measure $S(Q,\omega)$ with high statistical precision over a range of Q values $15\leqslant Q \leqslant 29$ Å^{-1}. High precision over a wide Q range allows us to determine several parameters in model fits of $S(Q,\omega)$ to the data. Since $R(Q,\omega)$ is changing rapidly in this Q range, we can identify $R(Q,\omega)$ in the data. Particularly, we can separate it from n_0 and $n(\mathbf{k})$, which are independent of Q. In earlier measurements[38] we determined the momentum distribution in normal ^{4}He at $T=2.3$ K and found that $n(\mathbf{k})$ differs significantly from a Gaussian with high occupation of low $\mathbf{k}$ states. We also determined the condensate fraction n_0 in superfluid ^{4}He at $T=1.6$ K, finding $n_0=(6\pm2)\%$.[39] The $R(Q,\omega)$ at $T=1.6$ K and 2.3 K was found to be the same within experimental precision.[39] In the present paper, we add measurements at $T=0.5$ K, 1.3 K, and 3.5 K and analyze the data using an improved procedure which is the same at all T. We find $n_0(T)=n_0(0)[1-(T/T_\lambda)^\gamma]$ with $n_0(0)=(7.25\pm0.75)\%$ and $\gamma=5.5\pm1.0$ in the superfluid phase and $n_0=0$ in the normal phase using the same model. We find that $n^*(\mathbf{k})$ for states above the condensate in superfluid ^{4}He (excluding the condensate induced portions) is less sharply peaked than $n(\mathbf{k})$ in normal ^{4}He.

In Secs. II and III, we describe the theoretical background of the data analysis and the models used to represent $n(\mathbf{k})$ and $R(Q,\omega)$. The data collection and reduction procedures are described in Sec. IV. The results are presented and discussed in Secs. V and VI, respectively.

II. THEORY AND ANALYSIS

In this section we describe the method used to analyze the data and extract the condensate fraction, the momentum distribution, and the FS broadening function. We begin with the expressions for the dynamic structure factor on which the method is based. The method consists, essentially, of cumulative expansion of the intermediate DSF and fitting the expanded DSF to the data to obtain the expansion coefficients. In this way, empirical expressions for the components of the DSF are obtained. We fit the same expressions *at all T both above and below* T_λ. The method was set out in detail by Glyde[6,40] and was discussed recently in a similar context by Azuah *et al.*[39]

At high wave vector transfer, where the static structure factor $S(Q)$ has saturated to $S(Q)=1$, the observed DSF $S(Q,\omega)$ reduces to the incoherent DSF

$$S_i(Q,\omega)=\frac{1}{2\pi}\int_{-\infty}^{\infty}dte^{i\omega t}S_i(Q,t). \tag{4}$$

At constant Q, $S_i(Q,\omega)$ is a broad peak in ω centered at ω_R with width proportional to v_R where, as in Eq. (1), $\omega_R=\hbar Q^2/2m$ and $v_R=\hbar Q/m$ are the free atom recoil energy and velocity, respectively. $S_i(Q,\omega)$ and $S_i(Q,t)$ can be scaled to approximately Q-independent forms if ω and t are replaced by the y scaling variable $y=(\omega-\omega_R)/v_R$ and its conjugate length $s=v_Rt$, respectively. The nearly Q-independent forms are $J(Q,y)=v_RS(Q,\omega)$ and

$$J(Q,s)\equiv e^{i\omega_Rt}S_i(Q,t)=\left\langle T_s\exp\left[-i\int_0^s ds'k_Q(s')\right]\right\rangle. \tag{5}$$

In the second expression, useful at short times t (short $s=v_Rt$), $T_t(T_s)$ is the time ordering operator and $\hbar k_Q=\hbar(\mathbf{k}\cdot\hat{\mathbf{Q}})$ is the struck atom momentum along $\mathbf{Q}$. The Fourier transform (4) is then

$$J(Q,y)=\frac{1}{2\pi}\int_{-\infty}^{\infty}dse^{iys}J(Q,s). \tag{6}$$

We express all the present results in the form $J(Q,y)$. We note that $J(Q,s)$ depends solely on the momentum $\hbar k_Q$ of the struck atom projected along Q.

The IA is obtained by approximating $k_Q(s')$ by its initial value $k_Q(0)=k_Q$ for all s' in Eq. (5), i.e.,

$$J_{IA}(s)=\langle e^{-ik_Qs}\rangle. \tag{7}$$

This assumes that the struck atom momentum k_Q is constant and not changed from its initial value by interaction as the struck atom recoils (no final-state interactions). Since the one-body density matrix (OBDM) is defined as $n(\mathbf{r})=\langle\Psi^+(0)\Psi(\mathbf{r})\rangle/n=\langle e^{-i\mathbf{k}\cdot\mathbf{r}}\rangle$, where $n=N/V$, we see also that $J_{IA}(s)$ is the OBDM for displacements $\mathbf{r}=s\hat{\mathbf{Q}}$ projected along $\mathbf{Q}$. The Fourier transform of the OBDM is the momentum distributions $n(\mathbf{k})$. Thus,

$$J_{IA}(y)=\frac{1}{2\pi}\left\langle\int dse^{iys}e^{-ik_Qs}\right\rangle \tag{8}$$

$$=\int d\mathbf{k}n(\mathbf{k})\delta(y-k_Q)$$

is the momentum distribution $n(\mathbf{k})$ for a momentum variable y projected along $\hat{\mathbf{Q}}$, i.e.,

$$J_{IA}(y)=n(y)=\int dk_x dk_y n(k_x,k_y,y), \tag{9}$$

where the z axis is chosen along $\hat{\mathbf{Q}}$. $J_{IA}(y)=n(y)$ is denoted the longitudinal momentum distribution.

When interactions between the recoiling struck atom and its neighbors are important, the full $J(Q,s)$ in Eq. (5) can be formally expressed as[21]

$$J(Q,s)=J_{IA}(s)R(Q,s), \tag{10}$$

which, as in Eq. (2), defines the FS function $R(Q,s)$. The Fourier transform of Eq. (10) is

$$J(Q,y)=\frac{1}{2\pi}\int ds e^{iys}J_{IA}(s)R(Q,s). \tag{11}$$

Below we introduce models for the OBDM $J_{IA}(s)=n(s)$ and the FS function $R(Q,s)$ based on expressions (7) and (5), respectively.

III. MODEL $J_{IA}(s)$ AND $R(Q,s)$

The model OBDM $J_{IA}(s)$ and FS function $R(Q,s)$, that we use to fit to the data are described in detail by Glyde[40] and Azuah *et al.*[39] When a Bose system has a condensate, it is convenient to separate its properties into ''condensate'' and ''above the condensate'' components.[41,42,5–7] The component arising from the condensate contains the singular behavior—such as a sharp peak in the response functions, a δ function in $n(\mathbf{k})$, and a long range component in the OBDM. The states above the condensate contribute regular behavior characteristic of a normal fluid. Specifically, the condensate contributes ''off-diagonal long range order'' to $J_{IA}(s)$. This is a constant term in $J_{IA}(s)$ of magnitude n_0, the condensate fraction. Also, when there is a condensate, quasiparticles can be excited out of and into the condensate to states above the condensate. At low k, these quasiparticle excitations have a linear dispersion and in liquid ^{4}He are part of the coupled quasiparticle/phonon excitation. These excitations contribute a term $n_0 f(s)$ to $J_{IA}(s)$ which is also long range in s but not constant. The contribution from the states above the condensate is short range in s. This ''normal'' component, which we denote by $n^*(s)$, can be well described by a cumulant expansion of Eq. (7) in powers of s. The model OBDM containing these three components is

$$J_{IA}(s)=n(s)=n_0[1+f(s)]+A_1 n^*(s). \tag{12}$$

Here A_1 is a constant chosen so that $n(\mathbf{k})$ is normalized to unity $[J_{IA}(0)=1]$.

To specify $f(s)$, we note that the three-dimensional (3D) momentum distribution $n(\mathbf{k})$ obtained by Fourier transforming Eq. (12) is

$$n(\mathbf{k})=n_0[1+f(\mathbf{k})]+A_1 n^*(\mathbf{k}). \tag{13}$$

The coupling term $f(\mathbf{k})$ between $k=0$ and $k\neq 0$ states, which leads to enhanced occupation of low momentum states, has been derived in k space by expressing $n(\mathbf{k})$ in terms of the quasiparticle/phonon response function.[42,6,7] This gives

$$n_0 f(\mathbf{k})=\left[\frac{n_0 mc}{2\hbar(2\pi)^3 n}\frac{1}{|\mathbf{k}|}\coth\left(\frac{c\hbar|\mathbf{k}|}{2k_B T}\right)\right]e^{-k^2/(2k_c^2)}. \tag{14}$$

The term in square brackets in Eq. (14) is the derived expression valid at low k. We have multiplied the derived expression by a Gaussian function to cut off $f(\mathbf{k})$ at higher k since $f(\mathbf{k})$ must vanish before the end of the phonon region, $k\simeq 0.7$ Å^{-1}. We have selected $k_c=0.5$ Å^{-1}. A reasonable lower limit of k_c is $k_c=0.3$ so that $0.3\leqslant k_c\leqslant 0.7$ Å^{-1}. The $n_0 f(s)$ in Eq. (9) is obtained by Fourier transforming $n_0 f(\mathbf{k})$ numerically.

The $n^*(s)$ follows by expanding Eq. (7) in cumulants.[40] We retain terms up to s^6,

$$n^*(s)=\exp\left[-\frac{\overline{\alpha}_2 s^2}{2!}+\frac{\overline{\alpha}_4 s^4}{4!}-\frac{\overline{\alpha}_6 s^6}{6!}\right], \tag{15}$$

where

$$\overline{\alpha}_2=\langle k_Q^2\rangle,\quad \overline{\alpha}_4=\langle k_Q^4\rangle-3\langle k_Q^2\rangle^2,$$

$$\overline{\alpha}_6=\langle k_Q^6\rangle-15\langle k_Q^4\rangle\langle k_Q^2\rangle+30\langle k_Q^2\rangle^3$$

are cumulants of $n(s)$. The model $J_{IA}(s)$ therefore has four parameters n_0, $\overline{\alpha}_2$, $\overline{\alpha}_4$, and $\overline{\alpha}_6$ that are obtained by fitting to experiment. As noted, A_1 is determined by normalizing $n(\mathbf{k})$, i.e., requiring $n(s=0)=1$. A typical $J_{IA}(s)$ at $T=1.6$ K showing the three components n_0, $n_0[1+f(s)]$, and the full $n(s)$ is displayed in Fig. 1. At $s=0$, $f(0)=0.28$ and $f(s)$ contributes approximates 15% of the condensate weight.

The model final-state function $R(Q,s)$ can be obtained by cumulant expansion of $J(Q,s)$ in Eq. (5) and the definition (10) (see Appendix A of Azuah *et al.*[39] and references therein for a full discussion). Up to powers s^6, this expansion is

$$R(Q,s)=\exp\left[\frac{i\overline{\beta}_3 s^3}{3!}+\frac{\overline{\beta}_4 s^4}{4!}-\frac{i\overline{\beta}_5 s^5}{5!}-\frac{\overline{\beta}_6 s^6}{6!}+\cdots\right]. \tag{16}$$

Expressions for the coefficients $\overline{\beta}_n$ are

$$\overline{\beta}_3=\overline{a}_3/\lambda Q,$$

$$\overline{\beta}_4=\overline{a}_4(\lambda Q)^2,$$

$$\overline{\beta}_5=\overline{a}_{52}/(\lambda Q)^3+\overline{a}_{54}/\lambda Q, \tag{17}$$

$$\overline{\beta}_6=\overline{a}_{62}/(\lambda Q)^4+\overline{a}_{64}/(\lambda Q)^2,$$

where the $\overline{a}_n$ are independent of Q and $\lambda=\hbar^2/m=1.0443$ meV Å^2 in liquid ^{4}He.

Expressions for the $\overline{a}_n$ can be obtained from the moments of $J(Q,y)$ and results up to $\overline{a}_{64}$ have been derived.[40,22] The lowest two are $\overline{a}_3=\langle\nabla^2 v(r)\rangle/6$ and $a_4=\langle(\nabla v)^2\rangle/3$ where

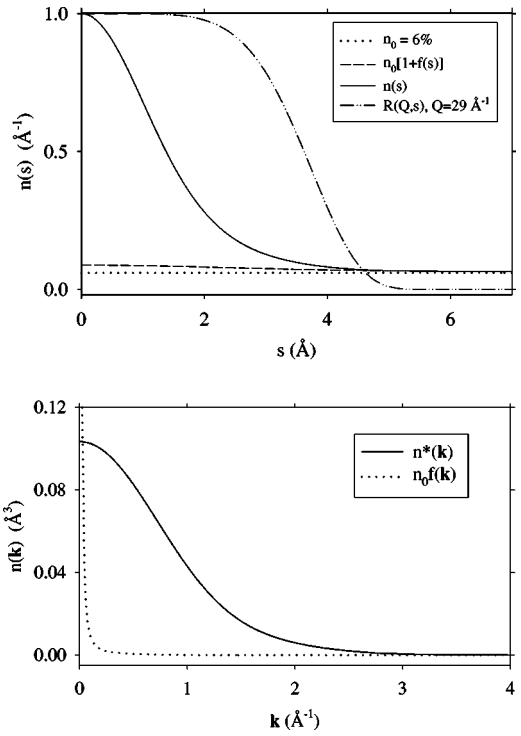

FIG. 1. Upper frame: Model one-body density matrix $n(s)=n_0[1+f(s)]+A_1n^*(s)$, (solid line) showing the components n_0 (dotted line), and $n_0[1+f(s)]$ (dashed line) for $n_0=6\%$ and $n^*(s)$ in Eq. (15) with $\bar{\alpha}_2=0.884$ Å^{-2}, $\bar{\alpha}_4=0.47$ Å^{-4}, and $\bar{\alpha}_6=1.03$ Å^{-6} obtained from fits to data at $T=1.6$ K (see Table I). $R(Q,s)$ (in Å^{-1}) is the FS function (16) for $Q=29$ Å^{-1}. Lower frame: The corresponding $n^*(\mathbf{k})$ and $n_0f(\mathbf{k})$ in momentum space.

$v(r)$ is the total potential experienced by the struck atom. The moments $\bar{R}_n=\int dy y^n R(Q,y)$ of $R(Q,y)$ are $\bar{R}_n=\bar{\beta}_n$ up to $n=5$. Given the Q dependence of the $\bar{\beta}_n$, clearly $R(Q,s)\rightarrow 1$ for $Q\rightarrow\infty$ and the IA is obtained at $Q\rightarrow\infty$.

We treat the $\bar{\beta}_n$ as parameters to be determined by fits to data at each Q value. The dependence of $\bar{\beta}_n(Q)$ on Q therefore emerges from the fit to the data. We found that $\bar{\beta}_4$ was very small and we set $\bar{\beta}_4=0$ for simplicity. This appears to be an accidental zero in liquid ^{4}He since $\bar{\beta}_4$ was not negligible in liquid neon.[43] A calculation of $\bar{a}_4/\lambda$ confirms that $\bar{\beta}_4$ is small in helium.[39] The $R(Q,s)$ therefore has three parameters $\bar{\beta}_3$, $\bar{\beta}_5$, and $\bar{\beta}_6$. From the Q dependence of $\bar{\beta}_5(Q)$ that emerged from the fit, we found that the first term $\bar{a}_{52}/(\lambda Q)^3$ dominated the $\bar{a}_{54}/(\lambda Q)$ term and $\bar{a}_{54}(\lambda Q)$ could be neglected, while in $\bar{\beta}_6(Q)$ the second term $\bar{a}_{64}/(\lambda Q)^2$ dominated and $\bar{a}_{62}(\lambda Q)^4$ could be neglected. Again, these are empirical findings.

In summary, $J_{IA}(s)R(Q,s)$ has a total of seven parameters: n_0, $\bar{\alpha}_2$, $\bar{\alpha}_4$, and $\bar{\alpha}_6$ which determine the OBDM, $J_{IA}(s)$, and $\bar{\beta}_3$, $\bar{\beta}_5$, and $\bar{\beta}_6$ which determines the FS function $R(Q,s)$ with $\bar{a}_{54}$ and $\bar{a}_{62}$ found to be negligible.

IV. DATA COLLECTION AND REDUCTION

The measurements were carried out at the ISIS pulsed spallation neutron source at the Rutherford Appleton Laboratory in the United Kingdom. The instrument used was the high energy direct geometry chopper spectrometer MARI with incident energies up to 1000 meV possible. More than 900 ^{3}He gas detectors provide an almost continuous coverage of scattering angles ϕ between 3° and 135° in steps of 0.43°. This makes it possible to measure a large range in momentum and energy transfer in a single experimental scan. Due to the pulsed nature of the source, data collection is performed in time-of-flight (TOF) mode in which the time of arrival of a neutron in the detector, measured from when the neutrons leave the moderator, determines its energy loss or gain after scattering from the sample. The momentum transfer depends on the TOF and the scattering angle of the neutron.

A high purity sample of ^{4}He gas was condensed into a cylindrical aluminum can of length 5.5 cm and diameter 6 cm placed inside a standard ^{3}He ''SORPTION'' cryostat. To minimize multiple scattering of neutrons within the sample, the cylindrical sample volume was split into six smaller cylindrical sections using highly neutron absorbing boron nitride disks. Sample temperatures were determined using a calibrated germanium resistance sensor and controlled using a Lakeshore temperature controller which achieved temperature stabilities of 0.01 K or better. Measurements were made at sample temperatures of 0.5, 1.3, 1.6, 2.3, and 3.5 K and at saturated vapor pressure (SVP). A second data set at 1.6 K and 2.3 K was also collected at an earlier time when the instrument was in a particularly stable condition and so these temperatures were chosen to perform the Q-dependent analysis. As an independent check, the resistance thermometry readings were compared to the vapor pressure readings of the sample. In order to cover the (Q,ω) range of interest, an incident neutron energy of 755 meV was employed. A measurement was also made with the sample cell empty to determine the sample-independent background scattering.

The collected data in TOF were then converted to energy transfer $(\hbar\omega)$ at constant scattering angle using standard procedures. The reader is referred to the recent article by Andersen *et al.*[44] for a detailed discussion of the data transformation from TOF to $S(\phi,\omega)$ and then to $S(Q,\omega)$.

In this article we have made use of the inherent scaling property of the scattering function with Q in the IA generally known as y scaling and referred to in the last section. In the IA, the scattering function can be portrayed as the longitudinal momentum distribution $J_{IA}(y)$ and does not depend on Q and ω separately. However, at moderate Q where the IA does not apply, y scaling is still approximately observed and it is useful to present the data as a generalized longitudinal momentum distribution $J(Q,y)=(\hbar Q/m)S(Q,\omega)$ (as discussed in Sec. II), which is weakly Q dependent as a result of FS effects. The experimental data were transformed to $J(Q,y)$ for $Q=20$ to 29 Å^{-1} in steps of 0.5 Å^{-1} and samples of the data are shown in Figs. 2 and 3. The statistical accuracy of the data is very high.

The observed $J(Q,y)$ consists of a convolution of the underlying momentum distribution, the FS function, and the instrumental resolution function. Hence, for a quantitative analysis of the data, the instrumental resolution function must be accurately known. We have used a Monte Carlo simulation method to calculate the instrumental resolution. In this method, the neutron scattering experiment is simu-

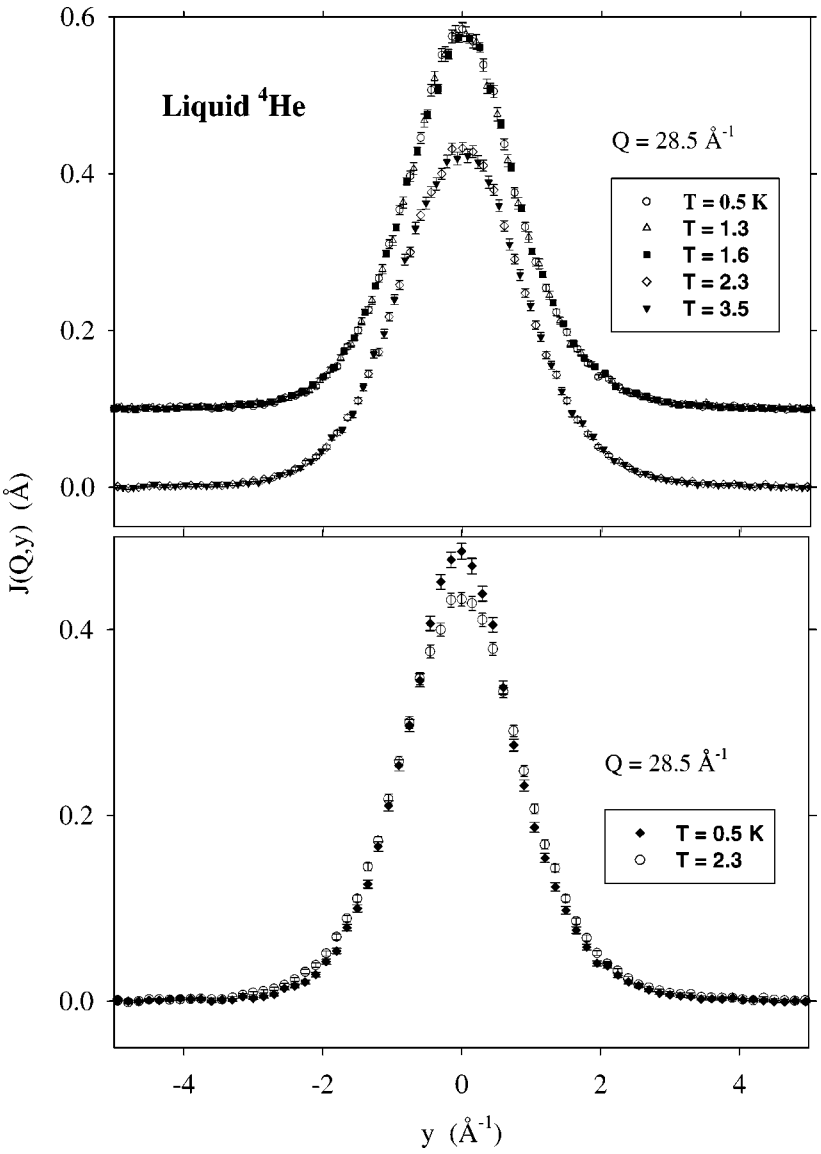

FIG. 2. Observed $J(Q,y)$ including the instrument resolution in liquid ^{4}He at SVP at the temperatures indicated. Upper frame shows that $J(Q,y)$ is similar at $T=2.3$ and $T=3.5$ K in normal ^{4}He and similar at $T=0.5$ K, 1.3 K and 1.6 K in superfluid ^{4}He. The lower frame shows that $J(Q,y)$ is very different in superfluid and normal ^{4}He ($T_\lambda=2.17$ K). $J(q,y)$ in the superfluid shows direct evidence of the condensate term $n_0R(Q,y)$: an increased peak height at $y=0$ and a right-left asymmetry around $y=0$.

lated using the known instrument parameters, sample cell geometry, and an estimate for the sample scattering function. The incident neutron beam characteristics were modeled using the Ikeda-Carpenter[45] speed and time distribution function with the adjustable parameters determined from a fit to the experimental monitor peaks before and after the sample. The simulation results are obtained in TOF and are then treated in the same way as the experimental data. The result is a convolution between the instrumental resolution function $I(Q,y)$, and the model scattering function input to the simulation. $I(Q,y)$ is then simply deconvoluted from the simulation. The resulting instrumental resolution function is shown as a dashed line in the top left frame of Fig. 3. We observe that $I(Q,y)$ narrows significantly with increasing Q and is quite small at large Q, thus increasing the reliability of the data.

V. RESULTS

The dynamic structure factor $J(Q,y)=v_RS(Q,\omega)$ was determined at 28 Q values in the range $15\leqslant Q\leqslant 29$ Å at five temperatures $T=0.5$ K, 1.3 K, 1.6 K, 2.3 K, and 3.5 K. Figure 2 shows the observed $J(Q,y)$ at $Q=28.5$ Å^{-1} as a function of energy transfer, y, including the instrument resolution function (see Fig. 3). In the upper frame, the $J(Q,y)$ at the three temperatures $T=0.5$ K, 1.3 K, and 1.6 K in the superfluid phase ($T<T_\lambda=2.17$ K) are shown together. These $J(Q,y)$ are clearly all very similar. At $T=0.5$ K $J(Q,y)$ is slightly higher in the peak region, $y=0$, where the term $n_0R(Q,y)$ makes its largest contribution. This reflects the somewhat larger condensate fraction at $T=0.5$ K. The two $J(Q,y)$ in normal ^{4}He at $T=2.3$ and 3.5 K are plotted together and are also very similar to each other. The peak height at 3.5 K is slightly lower, reflecting a small broaden-

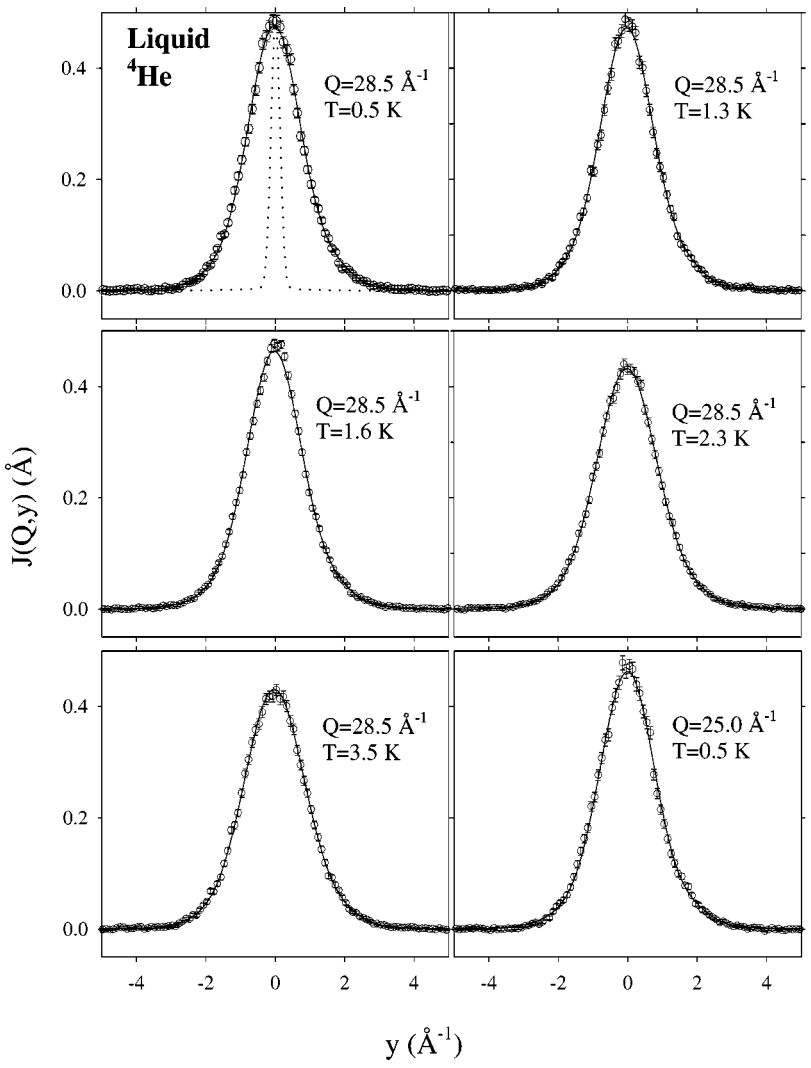

FIG. 3. Data with fits of the model $J(Q,y)$ given by Eqs. (11), (12), and (16) (solid lines) to the data. The dotted line is the MARI instrument resolution function.

ing of $n(\mathbf{k})$ between $T=2.3$ K and 3.5 K.

In the lower frame of Fig. 2, $J(Q,y)$ at $T=0.5$ K and $T=2.3$ K are plotted together. There we see a marked difference in the $J(Q,y)$ between these two temperatures arising from the condensate term $n_0R(Q,y)$ at $T=0.5$ K, which is absent in the normal phase. While $n_0R(Q,y)$ contributes predominantly at the peak ($y=0$), it also contributes in the wings of $J(Q,y)$. This leads to right-left asymmetry in $J(Q,y)$ around $y=0$ at $T=0.5$ K relative to $J(Q,y)$ at 2.3 K. For example, at $y\simeq 1.0$ Å^{-1} the right-hand side (RHS) of $J(Q,y)$ at 0.5 K is lower than the LHS relative to the 2.3 K $J(Q,y)$. At $y\simeq 2.5$ Å^{-1}, the RHS of $J(Q,y)$ at 0.5 K is higher than the LHS relative to the 2.3 K case. This asymmetry at 0.5 K reflects the asymmetry in $R(Q,y)$. The longitudinal momentum distribution $n(y)$ is an even function of y and must be symmetric about $y=0$. At 2.3 K, all of $R(Q,y)$ is folded with the much broader $n(y)$ and this smears out asymmetric features over wide y intervals in $J(Q,y)$ so that they cannot be seen. At $T=0.5$ K the $n_0R(Q,y)$ term appears ''unfolded'' and the asymmetry in $R(Q,y)$ can be seen in the data. In this way, the data show directly features expected for a condensate.

Figure 3 shows the observed $J(Q,y)$ at 28.5 Å^{-1} (and 25.0 Å^{-1}) along with the fit of the model $J(Q,y)$ from Eqs. (11), (12), and (16) as solid lines. The dotted line is the MARI instrument resolution function, which is narrow relative to both $J(Q,y)$ and $R(Q,y)$. Both the data and the fitted model $J(Q,y)$ include the instrument resolution. The fits are excellent. In the superfluid phase the fitted $J(Q,y)$ lies marginally below the data in the peak region, $y=0$. Again, $n_0R(Q,y)$ contributes both in the peak region and away from the peak. Since there are many points in the wings, the wings play an important role in determining $n_0R(Q,y)$. Apparently, the best fit total function at all y including $n_0R(Q,y)$ selects a combined $n^*(\mathbf{k})$, $R(Q,y)$, and n_0 that is somewhat low at $y=0$.

The seven fitted parameters obtained from fits to data at $T=1.6$ K for 19 Q values between $Q=20$ Å^{-1} and 29 Å^{-1} are shown in Fig. 4. The parameters are n_0, $\overline{\alpha_2}$, $\overline{\alpha_4}$, and $\overline{\alpha_6}$ which determine the OBDM $n(s)$ and $\overline{\beta_3}$, $\overline{\beta_5}$, and $\overline{\beta_6}$ which determine $R(Q,s)$. From Fig. 4(a), we see that the fitted values of n_0 are essentially independent of Q—as they should be. Similarly, we see in Fig. 4(b) that the fitted values of $\overline{\alpha_2}$, $\overline{\alpha_4}$, and $\overline{\alpha_6}$ are found to be independent of Q. The error bars shown are the error bars that

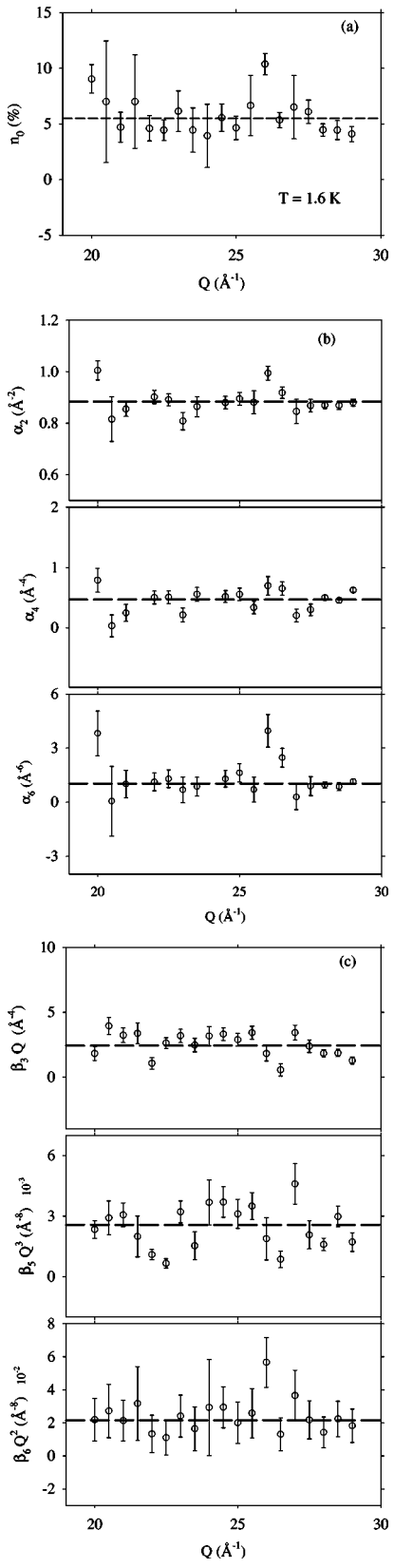

FIG. 4. Fitting parameters obtained from fits of the model $J_{IA}(s)R(Q,s)$ to data at $T=1.6$ K over a wide Q range giving final values $n_0=0.06\pm0.075$, $\overline{\alpha_2}=0.884\pm0.02$ Å^{-2}, $\overline{\alpha_5}=0.47\pm0.04$ Å^{-4}, $\overline{\alpha_6}=1.03\pm0.10$ Å^{-6} in $J_{IA}(s)$ and $\overline{a_3}/\lambda=2.43\pm0.25$ Å^{-4}, $\overline{a_{52}}/\lambda^3=2560\pm300$ Å^{-8}, and $\overline{a_{64}}/\lambda^2=215\pm25$ Å^{-8} in $R(Q,s)$. The fluctuation of the points with Q reflects the counting statistical error.

TABLE I. Parameters in the function $J(Q,s)=n(s)R(Q,s)$ given by Eqs. (12) and (16) obtained by fitting to data at $T=1.6$ K and 2.3 K ($\lambda=\hbar^2/m=1.0443$ meV Å$^2=12.12$ K Å^2). In the fits we found that $\overline{a_4}$, $\overline{a_{54}}$, and $\overline{a_{62}}$ in Eq. (17) were small (zero within statistical error) and set these coefficients to zero. The corresponding kinetic energies are $\langle K\rangle=14.45\pm0.3$, $\langle K\rangle=14.7\pm0.3$, and $\langle K\rangle=16.3\pm0.3$ K at $T=0.5$, 1.6, and 2.3 K, respectively.

T (K)	n_0 (%)	$\overline{\alpha_2}$ (Å^{-2})	$\overline{\alpha_4}$ (Å^{-4})	$\overline{\alpha_6}$ (Å^{-6})	$\overline{a_3}/\lambda$ (Å^{-4})	$\overline{a_{52}}/\lambda^3$ (Å^{-8})	$\overline{a_{64}}/\lambda^2$ (Å^{-8})
1.6	6.0 ± 0.75	0.884	0.47	1.03	2.43	2560	215
		±0.02	±0.05	±0.1	±0.25	±300	±25
2.3	0	0.897	0.46	0.38	3.3	2000	155
		±0.02	±0.05	±0.04	±0.3	±300	±20

emerge from the FRILLS fitting package that we use. These error bars are consistent with an independent determination of the error bars on an individual parameter as discussed in the Appendix and with the fluctuation of the parameters with Q.

Figure 4(c) shows the fitted $\overline{\beta_3}$, $\overline{\beta_5}$, and $\overline{\beta_6}$ values as functions of Q. We found $\overline{\beta_4}$ was small (zero within statistical error) and we set $\overline{\beta_4}=0$. From the upper frame, we see that the fitted $Q\overline{\beta_3}$ is independent of Q as expected from Eq. (17). The fitted value of $\overline{a_3}/\lambda=2.43\pm0.10$ Å^{-1} in $\overline{\beta_3}=\overline{a_3}/\lambda Q$ is shown as the dashed line in Fig. 4(c). From the fits, we find that $\overline{\beta_5}$ is dominated by its second term in Eq.

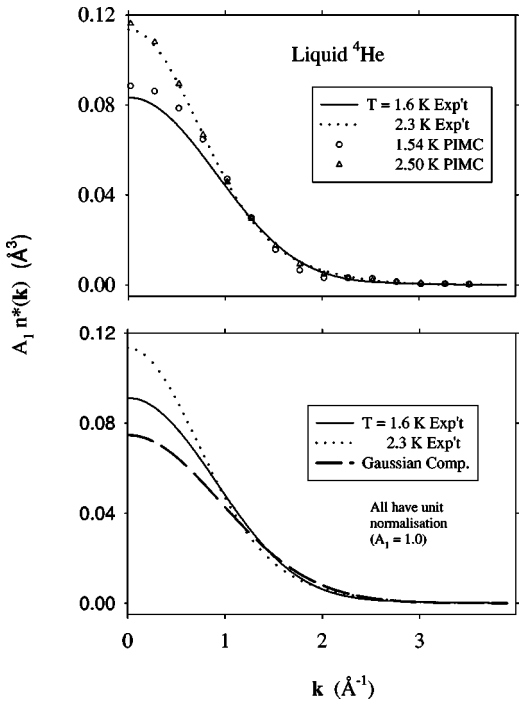

FIG. 5. Upper frame: Observed momentum distribution $A_1 n^*(\mathbf{k})$ *above* the condensate at $T=1.6$ K (solid line) and at $T=2.3$ K (dotted line). Open circles and open triangles are the corresponding quantities calculated by Ceperley and Pollock (Ref. 20) using PIMC methods at $T=1.54$ K and 2.50 K. Lower frame: Observed $n^*(k)$ at $T=1.6$ K and $T=2.3$ K both normalized to unity for comparison of the shape.

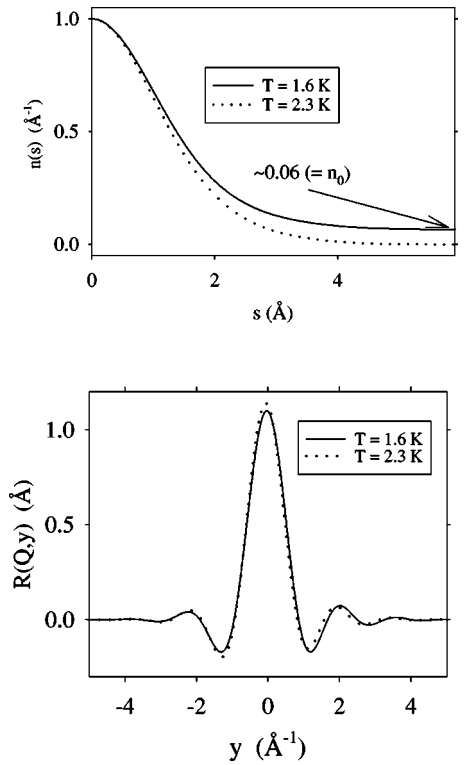

FIG. 6. Upper frame: Observed OBDM $n(s)$ at $T=1.6$ K and $T=2.3$ K. Lower frame: Observed final-state broadening function at $T=1.6$ K and $T=2.3$ K.

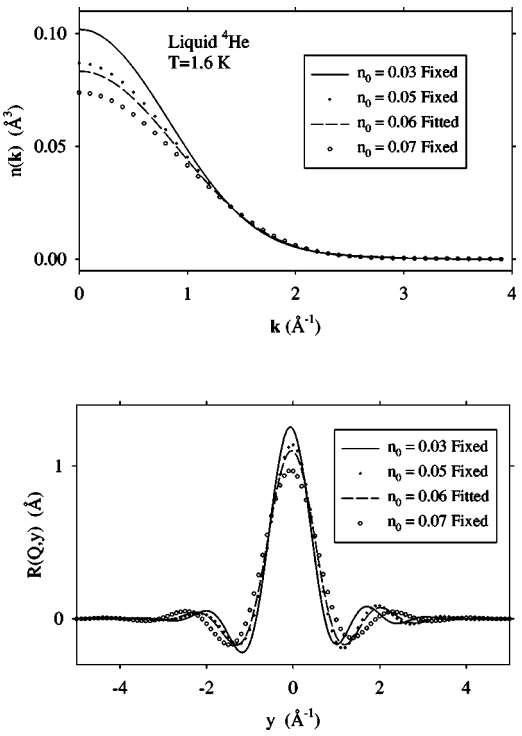

FIG. 7. Variation of the fitted $A_1 n^*(k)$ and $R(Q,y)$ functions for fixed input n_0 values showing the smooth variation of these fitted functions with n_0. The $n_0=0.06$ value gives the best overall fit (lowest χ^2).

(17), $\overline{\beta}_5=\overline{a}_{52}/(\lambda Q)^3$. That is, $\overline{\beta}_5 Q^3$ is largely independent of Q. Similarly, $\overline{\beta}_6$ is dominated by its first term in Eq. (17), since $\overline{\beta}_6 Q^2$ is independent of Q. While the plots in Fig. 4(c) display the Q dependence of $\overline{\beta}_n(Q)$ that emerge from the fits well, the $\overline{a}_n$ are most accurately obtained by plotting the $\overline{\beta}_n(Q)$ so that they have a slope and intercept. For example, a plot of $\overline{\beta}_6 Q^4=\overline{a}_{62}+\overline{a}_{64}Q^2$ vs Q^2 gives $\overline{a}_{64}$ as the slope and $\overline{a}_{62}$ as the intercept.

Values of the fitted parameters obtained from fits at the 19 largest Q values at temperatures of $T=1.6$ K and 2.3 K are listed in Table I. The data at the largest Q values are the most precise. Also, the data at $T=1.6$ K and 2.3 K are the most precise as discussed in Sec. IV, so that the parameters at these temperatures are quoted. The same model was fitted at all T. The calculation of the errors in the parameters is discussed in the Appendix.

The momentum distribution $A_1 n^*(\mathbf{k})$ for $\mathbf{k}$ values above the condensate calculated from the fitted parameters in superfluid ^{4}He at $T=1.6$ K and in normal ^{4}He at 2.3 K is shown in the upper frame of Fig. 5. At $T=2.3$ K, we find $n_0=(0\pm0.3)\%$ and $n^*(\mathbf{k})=n(\mathbf{k})$ $(A_1=1)$. Both $n^*(\mathbf{k})$ are much sharper than a Gaussian. The fitted $n(\mathbf{k})$ at $T=2.3$ K shown in Fig. 5 agrees with our previous determination.[38] The $A_1 n^*(\mathbf{k})$ at $T=1.6$ K (solid line) lies below the $T=2.3$ K $n(\mathbf{k})$ partly because $A_1\simeq0.93$. In the lower frame of Fig. 5 we have normalized $n^*(\mathbf{k})$ at both temperatures to unity so that the observed shape of $n^*(\mathbf{k})$ at $T=1.6$ and 2.3 K can be compared. The $n^*(\mathbf{k})$ is sharper in normal ^{4}He than in superfluid ^{4}He. The fraction that condenses into the $k=0$ state below T_λ appears to come from the low k states in $n^*(\mathbf{k})$ just above T_λ. We emphasize that the $n_0 f(\mathbf{k})$ term is not included in Fig. 5.

The path integral Monte Carlo (PIMC) $n^*(\mathbf{k})$ in normal ^{4}He (Ref. 20) is shown in the upper frame of Fig. 5 and agrees very well with our experimental $n^*(\mathbf{k})$, as noted initially by Azuah *et al.*[38] The agreement between PIMC and the present observed $n^*(\mathbf{k})$ is also good below T_λ. There is some discrepancy, much of which comes from a difference in normalization of $A_1 n^*(\mathbf{k})$ since the PIMC calculations find $n_0=8.5\%$ at $T=1.54$ K and we observe $n_0=6.0\%$ at $T=1.6$ K. There is no evidence of an $f(\mathbf{k})$ term in the PIMC results.

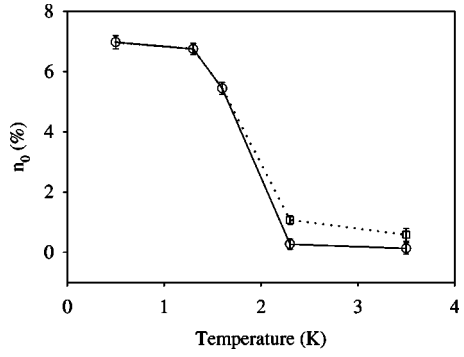

FIG. 8. Temperature dependence of $n_0(T)$. The circles are obtained using the present fitted $R(Q,y)$ for $T=1.6$ K (see Fig. 6) at all T, the fitted $n^*(k)$ for $T=1.6$ K below T_λ, and the $n(k)$ for $T=2.3$ K above T_λ. The squares are obtained as above but using $n^*(k)$ for $T=1.6$ K at all T. The error bars shown reflect the error in the T dependence only. The solid and dashed lines are guides to the eye.

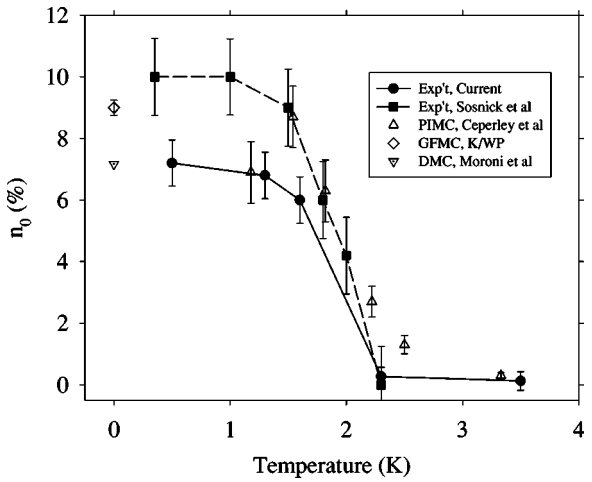

FIG. 9. Condensate fraction $n_0(T)$ observed here (full circles) and by Sosnick *et al.* (Ref. 34) (squares) compared with those calculated by Ceperley and Pollock (Ref. 20) (PIMC) and by Kalos *et al.* (Ref. 18) and Whitlock and Panoff (Ref. 19), Green function Monte Carlo (GFMC).

The upper frame of Fig. 6 shows the OBDM $n(s) = n_0[1+f(s)]+A_1 n^*(s)$ at $T=2.3$ K and $T=1.6$ K displaying the condensate term $n_0[1+f(s)]$ at 1.6 K, particularly. The FS function $R(Q,y)$ at these two temperatures is shown in the lower frame. Clearly, $R(Q,y)$ is effectively independent of temperature as expected for a function that depends on interactions in the fluid. We have used the 1.6 K $R(Q,y)$ in all further analysis.

To verify that n_0 is well determined in our fits with a total of seven parameters, we fixed n_0 at the values $n_0=0.03$, 0.05, and 0.07 and refitted for $n^*(\mathbf{k})$ and $R(Q,y)$ at $T=1.6$ K. The $A_1 n^*(\mathbf{k})$ and $R(Q,y)$ for these fixed values of n_0 are shown in Fig. 7. The $n^*(\mathbf{k})$ and $R(Q,y)$ change smoothly and consistently with the n_0 value selected, showing that $n^*(\mathbf{k})$ and $R(Q,y)$ are reliably determined as a function of n_0 in a statistical sense. The converse should also be true. The lowest global χ^2 and best fit was obtained for $n_0=0.06$.

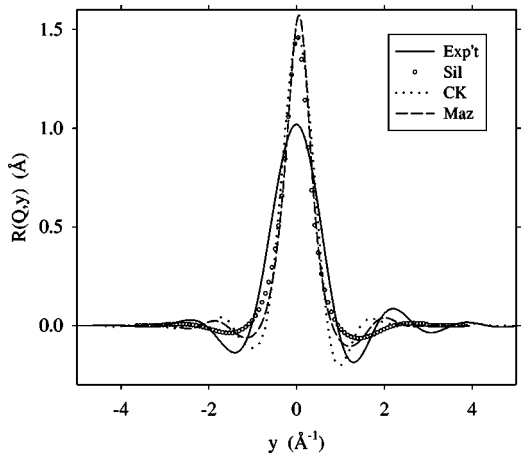

FIG. 10. Final-state broadening functions at $Q=23$ Å^{-1}: present observed (solid line), and calculated by Silver (Ref. 33) (open circles), by Carraro and Koonin (Ref. 46) (dotted line), and by Mazzanti *et al.* (Ref. 47) (dashed line).

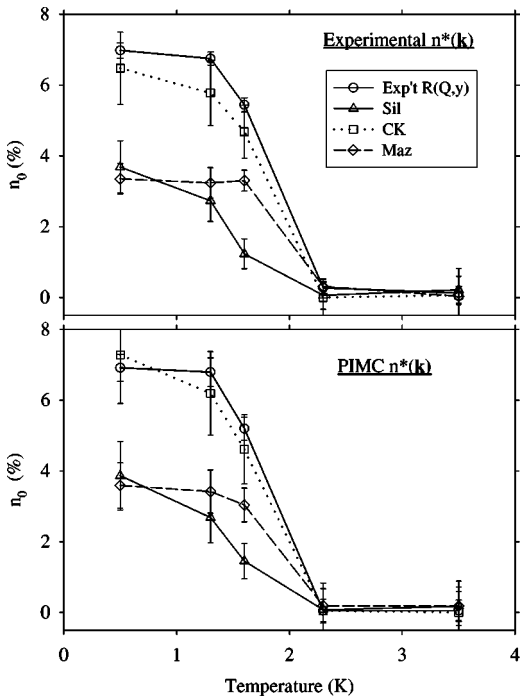

FIG. 11. Condensate fraction $n_0(T)$ obtained by fitting the present data using different FS functions $R(Q,y)$: the present observed $R(Q,y)$ (solid line and open circles), and $R(Q,y)$ calculated by Silver (solid line and triangles), by Carraro and Koonin (dotted line and squares), and by Mazzanti *et al.* (dashed line and squares). In the upper frame the present observed momentum distribution $n^*(\mathbf{k})$ is used ($T=1.6$ K) for $T<T_\lambda$, the present $n(\mathbf{k})$ ($T=2.3$ K) for $T>T_\lambda$. In the lower frame the PIMC $n^*(\mathbf{k})$ calculated by Ceperley and Pollock (Ref. 20) is used [$T=1.54$ K $n^*(\mathbf{k})$ for $T<T_\lambda$; $T=2.5$ K $n(\mathbf{k})$ for $T>T_\lambda$]. $n_0(T)$ is clearly sensitive to $R(Q,y)$ but not greatly sensitive to $n^*(\mathbf{k})$.

Using the best fit $R(Q,y)$ at $T=1.6$ K (see Fig. 6) at all temperatures we refitted to get $n_0(T)$ as a function of T. In the fit, $n^*(\mathbf{k})$ shown in Fig. 5 for $T=1.6$ K was used for $T<T_\lambda$ and $n^*(\mathbf{k})$ for $T=2.3$ K was used for $T>T_\lambda$. The resulting $n_0(T)$ are shown by the open circles in Fig. 8. The squares in Fig. 8 were obtained in the same way except the $n^*(\mathbf{k})$ obtained for $T=1.6$ K was used at all T, $T>T_\lambda$ and $T<T_\lambda$. Clearly a smooth $n_0(T)$ is obtained. Also we find $n_0=0$ in normal ^{4}He even if $n^*(\mathbf{k})$ at $T<T_\lambda$ is used. The error bars on $n_0(T)$ in Fig. 8 are the statistical error in the T dependence of $n_0(T)$ only. At $T=0.5$ K we find $n_0=(7.2\pm0.5)\%$ (see the Appendix) and a fit to the T dependence gives

$$n_0(T)=n_0(0)[1-(T/T_\lambda)^\gamma] \tag{18}$$

with $n_0(0)=(7.25\pm0.75)\%$ and $\gamma=5.5\pm1.0$.

Finally, Fig. 9 compares the present $n_0(T)$ shown in Fig. 8 (see parameters in Table I) with Monte Carlo (MC) values and previous measurements by Sosnick *et al.*[34] As noted the total error in the present n_0 is $\pm0.75\%$ (see the Appendix). These values are discussed below.

VI. DISCUSSION

From fits to data, we have obtained a condensate fraction of $n_0=(7.25\pm0.75)\%$ at $T=0$ K and the T dependence of

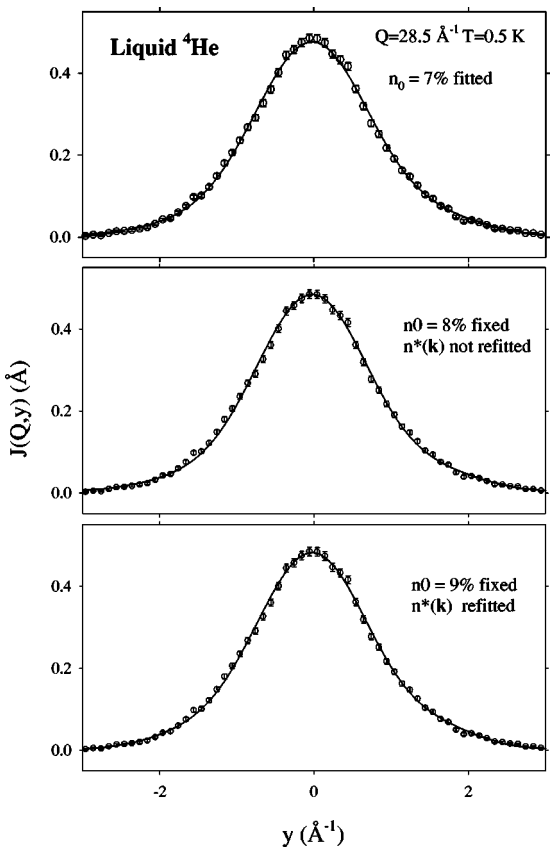

FIG. 12. Data at $Q=28.5$ Å^{-1} and $T=0.5$ K (open circles) with fitted $J(Q,y)$ given by Eqs. (10), (11), (12), and (16) (solid line). Upper frame: best overall fit giving lowest χ^2 and $n_0=(7.00\pm0.78)\%$. Middle frame: n_0 reset at $n_0=8\%$ to fit in peak region alone with other parameters unchanged. Lower frame: n_0 preset at $n_0=9\%$ and $n^*(k)$ refitted.

$n_0(T)$ shown in Fig. 9. This compares with $(10\pm1.25)\%$ found by Sokol and collaborators and $(9\pm0.01)\%$ at $T=0$ K calculated by Whitlock and Panoff[19] and by Kalos *et al.*[18] using GFMC methods. Ceperley and Pollock[20] using PIMC methods find $[(8-9)\pm1]\%$ at low T and the temperature dependence shown in Fig. 9.

We fitted the same model momentum distribution, $n_0[\,\delta(\mathbf{k})+f(\mathbf{k})]+A_1 n^*(\mathbf{k})$, to the data at all T, where n_0 is the fitted condensate fraction and A_1 follows from normalizing $n(\mathbf{k})$. In normal ^{4}He, we found $n_0=0$ with $A_1=1$ and $n^*(\mathbf{k})$ for states k above the condensate at $T=2.3$ K the same as determined previously.[38] This $n^*(\mathbf{k})$ in normal ^{4}He broadens only marginally between $T=2.3$ K and $T=3.5$ K. In normal ^{4}He, $n^*(\mathbf{k})$ shows a large occupation of low k states and is much more sharply peaked at low k than a Gaussian, as might be expected in a cold quantum liquid. PIMC calculations of $n^*(\mathbf{k})$ agree well with our observed $n^*(\mathbf{k})$ (see Fig. 5) as noted previously.[38]

Below T_λ the fit gives a finite $n_0(T)$ and $A_1\simeq0.91$ at $T=0.5$ K. The fitted $n^*(\mathbf{k})$ at $T<T_\lambda$ is also not Gaussian but is not so sharply peaked at low k as in normal ^{4}He. The high occupation of low k states in normal ^{4}He has apparently dropped in part into the condensate at $T<T_\lambda$. The fitted $n^*(\mathbf{k})$ at $T<T_\lambda$ also agrees well with the PIMC $n^*(\mathbf{k})$ although the PIMC result is slightly more sharply peaked. However, both PIMC calculations and the present observed

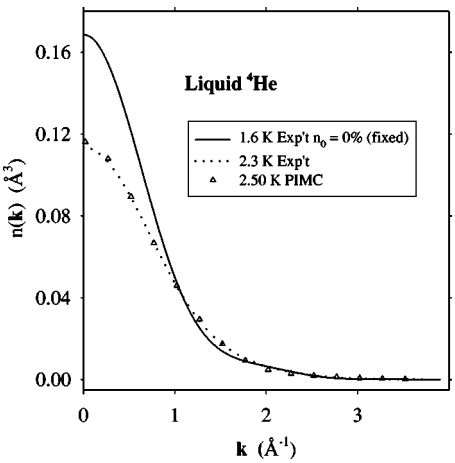

FIG. 13. Momentum distribution $n(\mathbf{k})$ obtained by fitting to data at $T=1.6$ K ($T<T_\lambda$) if n_0 is fixed at $n_0=0$ solid line. The dotted line is the corresponding $n(\mathbf{k})$ at $T=2.3$ K. The triangles are calculated (PIMC) values (Ref. 20) at $T=2.5$ K.

$n^*(\mathbf{k})$ show a clear broadening of $n^*(\mathbf{k})$ as T is decreased through T_λ. Below T_λ, there is also the $n_0 f(\mathbf{k})$ component shown in Fig. 1 which contributes at very low k values.

We find that the value of $n_0(T)$ below T_λ obtained in our fits is not sensitive to reasonable variation of $n^*(\mathbf{k})$. For example, we find the same $n_0(T)$ using our fitted $n^*(\mathbf{k})$ for normal ^{4}He, the PIMC $n^*(\mathbf{k})$, and our fitted $n(\mathbf{k})$ for $T<T_\lambda$.

The term $n_0 f(\mathbf{k})$ coupling the condensate to states above the condensate is highly localized near $k=0$ and its Fourier transform $n_0 f(s)$ is long range in s (see Fig. 1). When convoluted with $R(Q,y)$ at the present Q values, this term cannot be distinguished from $n_0\delta(\mathbf{k})$. This term has a firm theoretical foundation[6,7,42] at low k (e.g., $k\lesssim0.2$ Å^{-1}) and must be included. However, its behavior at higher k is not well known. It must vanish by the end of the phonon region of the phonon-roton excitations ($k\simeq0.7$ Å^{-1}). We have added a Gaussian cutoff with parameter $k_c=0.5$ Å to bring $n_0 f(\mathbf{k})$ smoothly to zero by $k\simeq0.7$ Å^{-1}. With this k_c value $n_0 f(s)$ contributes approximately 15% to $n_0[1+f(s)]$ in the range $2.5\leqslant s\leqslant4.5$ Å over which n_0 is measured in the present method. Specifically, at $T=0.5$ K and $Q=28.5$ Å^{-1} shown in Fig. 2, n_0 increases from $n_0=(7.00\pm0.78)\%$ to $n_0=(8.10\pm0.95)\%$ if the $n_0 f(s)$ term is not included at all. If k_c is reduced from $k_c=0.5$ to $k_c=0.3$, n_0 increases to $n_0=7.3\%$. The latter sensitivity to k_c is included in the present quoted error of n_0. In PIMC calculations n_0 is determined by the height of $n(s)$ at large s. At large enough $s(s\geqslant6$ Å), $f(s)$ is small and does not contribute to this height. The essential issue is that $n_0 f(s)$ does contribute to $n_0[1+f(s)]$ in the range $2.5\leqslant s\leqslant4.5$ Å that we can access in experiment to determine n_0, and it must be included.

To test the sensitivity of $n_0(T)$ to the FS function $R(Q,y)$, we refitted those data using the present model $n(\mathbf{k})$ in Eq. (10) combined with the $R(Q,y)$ calculated by Silver,[33,26] by Carraro and Koonin,[46] and by Mazzanti *et al.*[47] The FS functions are shown in Fig. 10 and the $n_0(T)$ obtained using these functions are shown in Fig. 11. The upper frame of Fig. 11 shows $n_0(T)$ obtained for the four $R(Q,y)$ when the present observed $n^*(\mathbf{k})$ is used in $n(\mathbf{k})$. The lower

frame of Fig. 11 shows the $n_0(T)$ obtained when the PIMC $n^*(\mathbf{k})$ is used. Clearly, $n_0(T)$ does depend sensitively on the $R(Q,y)$ used.

The $R(Q,y)$ calculated by Carraro and Koonin[46] yields $n_0(T)$ values close to those obtained using the experimental $R(Q,y)$. However, $n_0(T)$ obtained using the Silver[33,26] and Mazzanti *et al.*[47] $R(Q,y)$ are much lower, $n_0 \leqslant 4\%$. In normal ^{4}He we find $n_0=0$ independent of the FS function used.

The calculated $R(Q,y)$ are narrower and have a higher peak at $y=0$ than our observed $R(Q,y)$. We believe that the width at half height of $R(Q,y)$ is an important factor in setting the corresponding n_0 value obtained—a narrow $R(Q,y)$ leads to a smaller n_0. For example, the Carraro and Koonin (CK) $R(Q,y)$ is somewhat broader in the half height region than the other two calculated $R(Q,y)$. Secondly, the accuracy of $R(Q,y)$ at large y where $R(Q,y)$ oscillates is very important. An accurate $R(Q,y)$ for $y \geqslant 1.5$ Å^{-1} is needed for $n_0 R(Q,y)$ to select its full value in the fit. The oscillations in the CK and our observed $R(Q,y)$ have similar amplitudes. Also, we found that the calculated $R(Q,y)$ all peaked at higher y values than the observed $J(Q,y)$. Since $n(y)$ is symmetric in y, the peak position of $J(Q,y)$ is set by $R(Q,y)$. If this position is not correct, a poor fit is obtained and the $n_0 R(Q,y)$ term does not assume its full value in the fit. The last two factors appear to be responsible for the low n_0 obtained for the Silver and the Mazzanti *et al.* $R(Q,y)$.

In contrast, the observed $R(Q,y)$ could be too broad near $y=0$. There is no clear impetus for a narrower $R(Q,y)$ except that the fits to data shown in Fig. 3 fall marginally below the data at $y=0$ for $T<T_\lambda$. Since the $n^*(k)$ agrees well with PIMC values, the low $J(Q,y)$ at $y=0$ probably results from $R(Q,y)$. In this case n_0 might be too large to compensate. To explore the connection with n_0, we replot the $Q=28.5$ Å^{-1} and $T=0.5$ K data refitted with different n_0 values in Fig. 12. The top frame shows the best fit (lowest χ^2) giving $n_0=7.00\%$. The middle frame shows the same fit with n_0 alone artificially increased to 8%. A change of n_0 of 1% provides good agreement at $y=0$ and gives the magnitude of possible error in n_0. However, if we increase n_0 further to 9% and refit $n^*(k)$, the fit again falls marginally below the data near $y=0$, as shown in the lower frame of Fig. 12. The chief point is that $n_0 R(Q,y)$ contributes at all y values, not just $y=0$. The n_0 follows from the best fit over the whole range of y values. The fact that the Carraro and Koonin[46] $R(Q,y)$, which has a high peak at $y=0$, and the observed $R(Q,y)$, which is much lower at $y=0$, give similar n_0 values supports this picture. A fit that is low at $y=0$ does not mean that n_0 is too low or too high, probably only that $R(Q,y)$ is somewhat too broad.

If we fix $n_0=0$ and refit the data in the superfluid phase to obtain $n(k)$ and $R(Q,y)$ it is possible to obtain a reasonable fit. However, the $n(k)$ obtained is unrealistic as shown in Fig. 13. A large change in $n(k)$ between $T=2.3$ K and $T=1.6$ K is required, for example. The $n(k)$ must sharpen dramatically at low k over a small temperature interval of 0.7 K between 2.3 K and 1.6 K. This would be most unexpected in a cold quantum liquid where the thermal contribution ($T \simeq 2$ K) is already small compared to the zero point energy (e.g., $\langle K \rangle \simeq 15$ K). Thus, while the data can always be fitted without a condensate, the result is physically unrealistic.

The present $R(Q,y)$ has three terms,

$$R(Q,s)=\exp\left[\frac{is^3}{3!}\frac{\overline{a}_3}{\lambda Q}-\frac{is^5}{5!}\frac{\overline{a}_{52}}{(\lambda Q)^3}-\frac{s^6}{6!}\frac{\overline{a}_{64}}{(\lambda Q)^2}\right] \quad (19)$$

and depends on three parameters $\overline{a}_3$, $\overline{a}_{52}$, and $\overline{a}_{64}$. As noted above, we found from the fits that $\overline{a}_4$, $\overline{a}_{54}$, and $\overline{a}_{62}$ in Eq. (17) were small (zero within statistical error) and we set these coefficients equal to zero. A fitted $R(Q,y)$ with only three terms may not be sufficiently flexible. To test this we increased the number of terms retained, up to s^{10}, independently of whether the coefficients could be meaningfully determined in a fit to data. We found that a significantly narrower $R(Q,y)$ was not obtained without also leading to unrealistic behavior of $R(Q,y)$ at large y. Thus the width of $R(Q,y)$ appears to be largely set by the functional form in Eq. (16).

The expansion of $R(Q,s)$ in Eq. (16) has the correct structure to satisfy the first six moments $\overline{R}_n = \int dy y^n R(Q,y)$, of $R(Q,y)$. In particular, the zeroth, first, and second moments $\overline{R}_0=1$, $\overline{R}_1=\overline{R}_2=0$ are automatically satisfied by Eq. (16) because there are no terms in s or s^2. To obtain the correct values of $\overline{R}_3=\overline{\beta}_3=\overline{a}_3/\lambda Q$ and $\overline{R}_4=\overline{\beta}_4=\overline{a}_4/(\lambda Q)^2$ requires that the correct values of $\overline{a}_3$ and $\overline{a}_4$ emerge from the fit. We find $\overline{a}_3/\lambda = 2.5 \pm 0.2$ Å^{-4} from our fit compared with a value $\overline{a}_3/\lambda = 5.1 \pm 0.5$ Å^{-4} calculated using PIMC methods[39] and a value $\overline{a}_3/\lambda = 5.55$ Å^{-4} calculated by Rinat *et al.*[48] The coefficient $\overline{a}_3$ is somewhat below the expected value. In the fit, there is some compensation between $\overline{\beta}_3$ and $\overline{\beta}_5$. Similarly, the fitted value of $\overline{a}_4/\lambda^2$ is in reasonable agreement but somewhat below the calculated value.[39] While the present $R(Q,y)$ satisfies many moment relations and provides an excellent representation of FS effects, the three terms retained up to s^6 appear to simulate higher power terms not retained in the series. That is, the values of the coefficients adjust to best reproduce the whole series. Thus, while the function $R(Q,y)$ is well represented, the coefficient of each term in the truncated series may not correspond to the value expected if the whole series were retained.

We recently became aware of the extensive diffusion Monte Carlo calculations of liquid helium by Moroni *et al.*[50] They find a condensate fraction of $n_0=7.17\%$ at $T=0$ K and SVP, lower than previous MC values but in excellent agreement with the present observed value. Their momentum distribution and OBDM are similar to those found here but $n(\mathbf{k})$ has a ''shoulder'' at approximately $k \simeq 2$ Å^{-1} that is not observed here.

VII. CONCLUSION

The present results show that there is definitely a condensate in superfluid ^{4}He. This is demonstrated by the clear asymmetry of the observed $J(Q,y)$ about $y=0$ seen in the superfluid phase but not seen in the normal phase (see Fig. 2). This asymmetry arises from the term $n_0 R(Q,y)$ in $J(Q,y)$ that appears when there is a condensate. Using the same model to fit the data above and below T_λ we find a finite n_0 below T_λ and $n_0=0$ above T_λ, independent of mo-

mentum distribution $n^*(k)$ and final-state function $R(Q,y)$ used—although n_0 below T_λ is small when some calculated $R(Q,y)$ are used. Finally, a fit to the data in the superfluid without a condensate leads to a large and unrealistic change in $n(\mathbf{k})$ between $T=2.3$ K (above T_λ) and $T=1.6$ K (below T_λ) (see Fig. 13). The condensate is also reflected in the sensitivity of the results to $R(Q,y)$ below T_λ and the relative insensitivity to $R(Q,y)$ above T_λ.

A best fit to the data leads to $n_0(T)=n_0(0)[1-(T/T_\lambda)^\gamma]$ with $n_0(0)=(7.25\pm0.75)\%$ and $\gamma=5.5\pm1.0$. The statistical error on $n_0(0)$ is $\pm0.3\%$ with the remainder of the error arising from uncertainty in the sharply peaked component of the momentum distribution; the $n_0 f(\mathbf{k})$ term in Eq. (13). This value is 30% below previously accepted values.[25,34–37] It agrees with a recent diffusion Monte Carlo value,[50] is consistent with PIMC values[8,20] at finite T, but is lower than previous $T=0$ K Monte Carlo[19,20] values, which predict $n_0(0)=9.0\%$.

The shape of the momentum distribution $n^*(\mathbf{k})$ was determined in both phases and has much higher occupation of low k states than a classical, Gaussian $n(\mathbf{k})$. The $n^*(\mathbf{k})$ broadens somewhat as T is lowered below T_λ—as if some of the low momentum occupation in the normal phase drops into the condensate in the superfluid phase. The final-state function $R(Q,y)$ was determined from the data. We find that it is largely independent of temperature and the same in normal and superfluid ^{4}He within precision (see Fig. 6). The Fourier transform $R(Q,s)$ appears in Eq. (17) with parameter values listed in Table I. This expression can be used to obtain $R(Q,y)$ at higher or lower Q values. It is less sharply peaked near $y=0$ than most calculated $R(Q,y)$ and shows oscillations at larger y values needed to satisfy the moment relations. The condensate fraction obtained is the same or smaller when calculated $R(Q,y)$ are used in the data analysis.

ACKNOWLEDGMENTS

We thank Dr. F. Mazzanti for sending us his calculated $R(Q,y)$ and Dr. S. M. Bennington for valuable scientific and technical assistance. Valuable discussions on statistical errors with Dr. D. S. Sivia are gratefully acknowledged. This work was supported in part by the National Science Foundation through Research Grant Nos. INT-9314661 and DMR-9623961 and by the U.K. Engineering and Physical Science Research Council. We acknowledge the scientific support of the staff at the ISIS facility.

APPENDIX

In this appendix we discuss how the errors in the fitting parameters $n_0, \overline{\alpha_2}, \overline{\alpha_4}, \overline{\alpha_6}, \overline{a_3}, \overline{a_{54}}, \overline{a_{62}}$ listed in Table I are established. First, the error bars shown in Fig. 4 on these parameters at a given Q value are errors calculated by the fitting program FRILLS that was used to find the values of the parameters themselves. These error bars reflect the statistical error σ_i in the observed data points, $d_i=J_{\rm obs}(Q,y_i)\pm\sigma_i$.

As a check, we determined the errors at a given Q independently from the mean square deviation χ^2 of the data points d_i from the fitted function $j_i=J(Q,y)$. We define χ^2 as

$$\chi^2=\frac{1}{N_p}\sum_i^N\left(\frac{d_i-j_i}{\sigma_i}\right)^2$$

where $N_p=N-M+1$, N is the number of data points, M is the number of fitting parameters, and σ_i is the statistical error of d_i. The best fit values of the parameters in the function $j_i=J(Q,y)$ are those that minimize χ^2. If the fit of j_i to the observed points d_i is good, the deviation of the d_i from the function j_i will arise largely from the statistical error σ_i (i.e., $d_i-j_i\simeq\sigma_i$). In this event, the minimum value χ^2_m of χ^2 will be $\chi^2_m\simeq1$.

If we assume that χ^2, as a function of the fitting parameters, is distributed as a Gaussian about the minimum value χ^2_m, then, when a parameter is moved one standard deviation away from its best value, χ^2 increases from χ^2_m to χ^2_m+1/N.[49] We can determine the standard deviation of a parameter, say n_0, by adjusting n_0 until χ^2 increases from χ^2_m to χ^2_m+1/N. For example, at $Q=27.5$ Å^{-1} and $T=1.6$ K this procedure gives a standard deviation of n_0 of $\pm1.15\%$. In this case $\chi^2_m=1.0175$, $\chi^2_m+1/N_p=1.0257$ ($N_p=122$) and it is important to readjust all other parameters as n_0 is changed. This error agrees well with the error $n_0=(6.10\pm1.06)\%$ calculated by FRILLS and shown in Fig. 4 at $Q=27.5$ Å^{-1}. We found a similar agreement of errors at other Q values, at other temperatures, and for other parameters. At some Q values the error is large because the data set was small.

The fluctuation of the parameters with Q (e.g., n_0) shown in Fig. 4 arises from the statistical error in determining the parameters. The magnitude of this fluctuation can also be used to determine the statistical error in the parameters. For example, one standard deviation of the parameter value should cover 68% of the points shown in Fig. 4. In the case of n_0, $n_0=(5.7\pm1.2)\%$ readily covers 70% of the points in Fig. 4(a). This determination of the statistical error of n_0 agrees well with the other two determinations noted above in most cases.

We have used the fluctuation of the parameters with Q shown in Fig. 4 to determine their error. Since there are N_Q values of Q, we may divide this error on the parameter by $\sqrt{N_Q}$. This gives ($N_Q=19$), for example, $n_0=(5.7\pm0.3)\%$ or a standard deviation of $\sigma=0.3\%$. Similarly, we obtain $\alpha_2=0.884\pm0.01$. In a previous paper[39] we determined the error from the fluctuation of the parameter with Q but did not divide by $\sqrt{N_Q}$.

As noted in the text the function $f(k)$ contains a cutoff parameter k_c which is not known with certainty. This uncertainty adds an additional error (to n_0 especially). We may incorporate this uncertainty in the error of n_0 as follows. The k_c lies in the range $0.3\leqslant k_c\leqslant0.7$ Å^{-1} with perceived best value $k_c=0.5$ Å^{-1}. At $Q=27.5$ Å^{-1} and $T=1.6$ K, we find n_0 varies from $n_{0H}=(6.37\pm1.12)\%(k_c=0.3)$ to $n_{0L}=(6.10\pm1.03)\%(k_c=0.7)$. This is a typical change with k_c. Assuming that the standard deviation σ of both n_{0H} and n_{0L} is the same as obtained above for $n_{0C}=5.7\%(k_c=0.5)$ (i.e., $\sigma=0.3$), the n_0 values range from $n_{0L}-\sigma<n_0<n_{0H}+\sigma$. This gives an average value $n_{0M}=[(n_{0H}+\sigma)+(n_{0L}-\sigma)]/2=5.9\%$ and spread $S=2\sigma_T=[n_{0H}+\sigma-(n_{0L}-\sigma)]$ or $\sigma_T=(n_{0H}-n_{0L})/2+\sigma\simeq0.5\%$. Including the uncertainty

in k_c, we obtain a condensate fraction $n_0 = n_{0M} \pm \sigma_T = (5.9 \pm 0.5)\%$ with a $\sigma_T = 0.5\%$ total standard deviation. When k_c is changed from $k_c = 0.5$ to 0.3, the best fit $\overline{\alpha_n}$ parameters change by approximately 1%. There is no change from $k_c = 0.5$ to 0.7. This procedure is an approximation to the general method of evaluating χ^2 as a function of k_c and n_0 and determining values of n_0 at which $\chi^2 = \chi^2_m + 1/N$ over the range $0.3 \leqslant k_c \leqslant 0.7$.

For n_0 we round the result to $n_0 = (6.0 \pm 0.75)\%$, allowing an additional error of 0.25% for error in the form of $f(\mathbf{k})$. The error $\pm 0.75\%$ arises from 0.3% statistical error and 0.45% for uncertainty in the function $f(\mathbf{k})$. It is less than the error quoted previously,[39] which was too large in both the statistical error and in the uncertainty arising from k_c. The present error arises predominantly from uncertainty in the $n_0 f(\mathbf{k})$ term.

[1] P. Kapitza, Nature (London) **141**, 74 (1938).
[2] J. F. Allen and A. D. Misener, Nature (London) **141**, 75 (1938); Proc. R. Soc. London, Ser. A **172**, 467 (1939).
[3] K. Mendelsshon, *The Quest for Absolute Zero*, World University Library (McGraw-Hill, New York, 1966).
[4] J. Wilks, *The Properties of Liquid and Solid Helium* (Clarendon Press, Oxford, 1967).
[5] P. Nozières and D. Pines, *Theory of Quantum Liquids, Vol. II: Superfluid Bose Liquids* (Addison-Wesley, Redwood City, CA, 1990).
[6] H. R. Glyde, *Excitations in Liquid and Solid Helium* (Oxford University Press, Oxford, 1994).
[7] A. Griffin, *Excitations in a Bose-Condensed Liquid* (Cambridge University Press, Cambridge, England, 1993).
[8] D. M. Ceperley, Rev. Mod. Phys. **67**, 279 (1995).
[9] M. H. Anderson, J. R. Ensher, M. R. Matthews, C. E. Wieman, and E. A. Cornell, Science **269**, 198 (1995).
[10] K. B. Davis, M.-O. Mewes, M. R. Andrews, N. J. van Druten, D. S. Durfee, D. M. Kurn, and W. Ketterle, Phys. Rev. Lett. **75**, 3969 (1995).
[11] C. C. Bradley, C. A. Sackett, J. J. Tolett, and R. G. Hulet, Phys. Rev. Lett. **75**, 1687 (1995).
[12] F. Dalfovo, S. Giorgini, L. P. Pitaevskii, and S. Stringari, Rev. Mod. Phys. **71**, 463 (1999).
[13] *Bose-Einstein Condensation*, edited by A. Griffin, D. W. Snoke, and S. Stringari (Cambridge University Press, Cambridge, England, 1995).
[14] A. Einstein, Sitzungsber. K. Preuss. Akad. Wiss., Phys. Math. Kl. **1924**, 261.
[15] S. N. Bose, Z. Phys. **26**, 178 (1924).
[16] F. London, Nature (London) **141**, 643 (1938); Phys. Rev. **54**, 947 (1938).
[17] O. Penrose and L. Onsager, Phys. Rev. **104**, 576 (1956).
[18] M. H. Kalos, M. A. Lee, P. A. Whitlock, and G. V. Chester, Phys. Rev. B **24**, 115 (1981).
[19] P. A. Whitlock and R. M. Panoff, Can. J. Phys. **65**, 1409 (1987).
[20] D. M. Ceperley and E. L. Pollock, Can. J. Phys. **65**, 1416 (1987).
[21] H. A. Gersch and L. J. Rodriguez, Phys. Rev. A **8**, 905 (1973).
[22] V. F. Sears, Phys. Rev. B **30**, 44 (1984), and references therein.
[23] A. Miller, D. Pines, and P. Nozières, Phys. Rev. **127**, 1452 (1962).
[24] P. C. Hohenberg and P. M. Platzman, Phys. Rev. **152**, 198 (1966).
[25] P. E. Sokol, in *Bose-Einstein Condensation* (Ref. 13).
[26] R. N. Silver and P. E. Sokol, *Momentum Distributions* (Plenum, New York, 1989).
[27] H. R. Glyde and E. C. Svensson, in *Neutron Scattering*, Vol. 23, Part B of *Methods in Experimental Physics*, edited by D. L. Price and K. Sköld (Academic Press, New York, 1987), p. 303.
[28] E. C. Svensson and V. F. Sears, in *Frontiers of Neutron Scattering*, edited by R. J. Birgeneau, D. E. Moncton, and A. Zilinger (North-Holland, Amsterdam, 1986).
[29] E. C. Svensson, Los Alamos Report No. LA-10227-C Vol. 2, p. 456, 1984 (unpublished).
[30] P. Martel, E. C. Svensson, A. D. B. Woods, V. F. Sears, and R. A. Cowley, J. Low Temp. Phys. **23**, 285 (1976).
[31] V. F. Sears, E. C. Svensson, P. Martel, and A. D. B. Woods, Phys. Rev. Lett. **49**, 279 (1982).
[32] H. A. Mook, Phys. Rev. Lett. **51**, 1454 (1983).
[33] R. N. Silver, Phys. Rev. B **39**, 4022 (1989).
[34] T. R. Sosnick, W. M. Snow, P. E. Sokol, and R. N. Silver, Europhys. Lett. **9**, 707 (1990).
[35] T. R. Sosnick, W. M. Snow, and P. E. Sokol, Phys. Rev. B **41**, 11 185 (1990).
[36] T. R. Sosnick, W. M. Snow, R. N. Silver, and P. E. Sokol, Phys. Rev. B **43**, 216 (1991).
[37] P. E. Sokol and W. M. Snow, in *Excitations in Two-Dimensional and Three-Dimensional Quantum Fluids*, Vol. 257 of *NATO Advanced Study Institute, Series B: Physics*, edited by A. F. G. Wyatt and H. J. Lauter (Plenum, New York, 1991).
[38] R. T. Azuah, W. G. Stirling, H. R. Glyde, P. E. Sokol, and S. M. Bennington, Phys. Rev. B **51**, 605 (1995).
[39] R. T. Azuah *et al.*, Phys. Rev. B **56**, 14 620 (1997).
[40] H. R. Glyde, Phys. Rev. B **50**, 6726 (1994).
[41] N. N. Bogoliubov, J. Phys. (Moscow) **11**, 23 (1947).
[42] J. Gavoret and P. Nozières, Ann. Phys. (N.Y.) **28**, 349 (1964).
[43] R. T. Azuah, W. G. Stirling, H. R. Glyde, and M. Boninsegni, J. Low Temp. Phys. **109**, 287 (1997).
[44] K. H. Andersen, W. G. Stirling, R. Scherm, A. Stunault, B. Fåk, A. Godfrin, and A. J. Dianoux, J. Phys. C **6**, 821 (1994).
[45] S. Ikeda and J. M. Carpenter, Nucl. Instrum. Methods Phys. Res. A **239**, 536 (1985).
[46] C. Carraro and S. E. Koonin, Phys. Rev. Lett. **65**, 2792 (1990).
[47] F. Mazzanti, J. Boronat, and A. Polls, Phys. Rev. B **53**, 5661 (1996).
[48] A. S. Rinat, M. F. Taragin, F. Mazzanti, and A. Polls, Phys. Rev. B **57**, 5347 (1998).
[49] D. S. Sivia, *Data Analysis: A Bayesian Tutorial* (Clarendon Press, Oxford, 1996).
[50] S. Moroni, G. Sentore, and S. Fantoni, Phys. Rev. B **55**, 1040 (1997).